Towards the measurement of the CKM angle γ using the Tree-level decay B –> D[hh]K*[Ksπ] at the LHCb experiment

Simon Nakhoul

UFR Sciences et Technologies

Laboratoire d'Annecy-le-Vieux de Physique des Particules

MASTER SCIENCES DE LA MATIERE
DEUXIEME ANNEE

SPECIALITE : Physique des Particules

RAPPORT DE STAGE

Towards the measurement of the CKM angle γ using the Tree-level decay B→D[hh]K[K_sπ] at the LHCb experiment*

par

Simon NAKHOUL

Responsables de stage : **Vincent TISSERAND**
Daniel DECAMP

Juin 2015

Advance, and never halt, for advancing is perfection. Advance and do not fear the thorns in the path, for they draw only corrupt blood.

[A visit from Wisdom]

by Khalil Gebran

Acknowledgment

I would like to start by thanking every single member of the LHCb collaboration at LAPP especially Vincent Tisserand for his assistance, patience and for giving me the chance to do this internship from which I learned a lot.
I extend my thanks also to Daniel Decamp, I really appreciated his Flavor physics lectures and it was a great honor to be one of his students for the first two weeks of this internship.
In addition, a thank you for all the interns and the PhD students at LAPP for their welcoming spirit and their efforts to include me in their activities.
I am deeply grateful to Stéphane Monteil responsible of the particle physics specialty at the Blaise Pascal University, who showed me nothing but kindness and guidance during the past two years.
Last but not least, my biggest thanks by far goes to my family: Dad, Mom, Zouz, Raby. Thank you for your support, unconditional love and most importantly for being there for me when I needed you the most.

Annecy 04/06/2015

Contents

1 Introduction

The Standard Model (SM) of particle physics is a theory of subatomic particles and how they interact. It combined all that was known about these particles and predicted the existence of additional particles as well. However, the SM is not enough to explain many phenomena, one of which the matter antimatter asymmetry observed in the universe. CP violation is thought to be responsible for this asymmetry. Nonetheless, the SM predicts only a small portion of the CP violation needed to explain this huge preference for matter over antimatter. This leads particle physicists to search for new CP violation sources in new physics (NP) beyond the SM. Currently, the LHCb experiment at the the Large Hadron Collider (LHC) accelerator at CERN is trying to shed a light on this problem. LHCb is explicitly dedicated for the study of CP violation and the indirect search for new physics in rare b-hadron decays.
One of the most difficult CP-violating parameters to measure at LHCb today is the CKM angle γ. This angle can be measured both via tree level processes (γ_{SM}) without any NP contributions and via loop processes which are sensitive to NP. The measurement of (γ_{SM}) with high accuracy is a crucial step towards the determination of the existence of NP. Not to mention, it can enhance our understanding of the CP violation within the SM. During this internship the tree-level decay $B \to DK^*$ was chosen for an attempt to measure the angle γ.
The next section 2 of this document, will provide details about CP violation, the CKM unitarity triangle, its angles and the methods used to extract γ. In section 3, the LHCb detector and its sub-detectors are briefly described. Finally, every step of the Data Analysis aspect of the work will be presented in sections 4 and 5.

2 Theoretical Context

2.1 CP violation

CP symmetry is a composite of two discrete symmetries: The charge conjugation symmetry C swapping the signs of all particle's charges and the Parity symmetry P transforming everything into its mirror image. These two symmetries are respected individually by the strong and electromagnetic interactions but maximally violated by the weak interaction.
C-symmetry violation could be illustrated by the following example. Suppose one applies charge conjugation transformation on a left handed neutrino; it produces a left handed anti neutrino. It's known that only right handed anti neutrinos and left handed neutrinos exist in nature. Since the neutrino interacts only weakly, it's clear that C-symmetry is maximally violated by the weak interaction. As for the P-symmetry, under a Parity transformation a left handed neutrino will become a right handed neutrino proving that parity just like charge conjugation is maximally

violated by the weak interaction.

Before the discovery of the exclusive existence of right handed anti neutrinos and left handed neutrinos. Parity violation was observed for the first time in 1956 in beta decays of ^{60}Co nuclei by Wu et al.[1]. They found that most of the electrons were emitted in the direction opposite to that of the spin of the ^{60}Co nuclei.

Following the violation of both symmetries, it was thought that the combination of the two (CP symmetry) is an exact symmetry for the weak interaction. As it turned out, even CP is violated in certain rare decays.

CP violation was discovered experimentally in the neutral Kaon system by J. Christenson et al. [2] in 1964. They observed the decay of the long-living neutral Kaon which usually decays into 3 pions final state with CP eigenvalue of -1, into two pions with a CP eigenvalue of $+1$.

in 2001, more than three decades later CP violation was established successfully for the first time in the B system at Babar [3] and Belle [4] experiments. CP violation can be manifested in three different ways:

CP violation in Decay: Also known as "direct CP violation", it occurs for both charged and neutral decays when the decay rate of a particle X to a final state f is not equal to that of its antiparticle $\overline{X}$:

$$\Gamma(X \to f) \neq \Gamma(\overline{X} \to \overline{f}) \tag{1}$$

Or in other words, when the two decay amplitudes defined as $A_f = \langle f|H|X\rangle$; $\overline{A}_{\overline{f}} = \langle \overline{f}|H|\overline{X}\rangle$ are different in modulus $|\frac{\overline{A}_{\overline{f}}}{A_f}| \neq 1$. This is the type of CP violation that will be studied during this internship.

CP violation in mixing: Also known as "indirect CP violation", this type is dedicated to CP violation within the neutral meson systems (K^0, D^0, B^0). It occurs when the probability of a particle oscillating to its antiparticle is different from the probability of an anti-particle oscillating to its particle.

$$P(X^0 \to \overline{X^0}) \neq P(\overline{X^0} \to X^0) \tag{2}$$

CP violation in interference between decay with or without mixing

This violation type appears when a particle and its antiparticle decay into the same final state and interference between the decay process and mixing occur. It could be simply translated by the following inequality:

$$\Gamma(X^0 \to \overline{X^0} \to f) \neq \Gamma(\overline{X^0} \to X^0 \to f) \tag{3}$$

2.2 CKM matrix

In attempt to preserve the universality of the weak interaction Cabibbo suggested in 1963 the mixing between down and strange quarks by introducing the Cabibbo mixing angle θ_c. This angle was the only parameter for the 2×2 real matrix called the Cabibbo mixing matrix. In 1970, Sheldon Lee Glashow, John Iliopoulos and Luciano Maiani introduced the GIM mechanism [5] to explain why flavor changing neutral currents (FCNC) and ($\Delta S = 2$) strangeness transitions in weak interaction are suppressed which led to the prediction of the existence of the charmed quark.

With the discovery of new quark flavors and the need to account for CP violation in the Standard Model, the Cabbibo matrix was generalized by Kobayashi and Maskawa into a 3×3 unitarity matrix called(Cabibbo Kobayashi Maskawa) CKM matrix [6]. The presence of at least three generations of quarks is required to integrate the CP violating complex phase in the CKM matrix which can be written in terms of nine elements. These elements represent every possible weak interaction coupling among quarks of the three families by exchanging a $W^{\pm}$ boson. The CKM matrix can be written as follows:

$$V = \begin{pmatrix} V_{ud} & V_{us} & V_{ub} \\ V_{cd} & V_{cs} & V_{cb} \\ V_{td} & V_{ts} & V_{tb} \end{pmatrix}$$

For example, V_{ub} represents the coupling between the up quark and the down quark. The couplings between anti quarks are given by the complex conjugates of the elements. The CKM matrix can be parameterized in a variety of ways. The most two common parameterizations are:

The standard parametrization

The PDG [7] describes the CKM matrix as follow:

$$V = \begin{pmatrix} c_{12}c_{13} & s_{12}c_{13} & s_{13}e^{-i\delta_{13}} \\ -s_{12}c_{23} - c_{12}s_{23}s_{13}e^{i\delta_{13}} & c_{12}c_{23} - s_{12}s_{23}s_{13}e^{i\delta_{13}} & s_{23}c_{13} \\ s_{12}s_{23} - c_{12}c_{23}s_{13}e^{i\delta_{13}} & -c_{12}s_{23} - s_{12}c_{23}s_{13}e^{i\delta_{13}} & c_{23}c_{13} \end{pmatrix}$$

where $c_{ij} = cos\Theta_{ij} s_{ij} = sin\Theta_{ij}$ for $i < j = 1, 2, 3$. This matrix is obtained after three successive rotations about different axes and by introducing a phase δ which is responsible for the CP violation in the Standard Model. The four independent parameters of the matrix are the three Euler angles which represent the mixing angles between the three quarks generations $\Theta_{12}, \Theta_{13}, \Theta_{23}$ and the complex phase δ.

The Wolfenstein parameterization

For this parameterization, the CKM matrix presents a hierarchical structure in which the elements on the diagonal are found to be close to unity, as for the non-diagonal elements the further they are from the diagonal the smaller in magnitude they get. As one can see in Figure 1-a, transi-

tions between quarks of the same generation are highly favored $O(1)$. Transitions between quarks from the first generation and the third generation (for instance the transition between the down quark and the top quark) are highly suppressed $O(\lambda^3)$. The transition to this parameterization could be established with the following substitutions: $\lambda \equiv s_{13}$; $A\lambda^2 \equiv s_{23}$; $A\lambda^3(\rho - i\eta) \equiv s_{13}e^{-i\delta}$.

$$V = \begin{pmatrix} 1 - \frac{\lambda^2}{2} & \lambda & A\lambda^3(\rho - i\eta) \\ -\lambda & 1 - \frac{\lambda^2}{2} & A\lambda^2 \\ A\lambda^3(1 - \rho - i\eta) & -A\lambda^2 & 1 \end{pmatrix} + O(\lambda^4)$$

The CKM matrix is characterized by the real parameters λ, A, ρ and η.
The elements of CKM are not predicted by the Standard Model, they are measured experimentally. Processes used to measure their magnitudes are presented in Figure1-b. For example $|V_{ub}|$ is measured via semileptonic B meson decays.

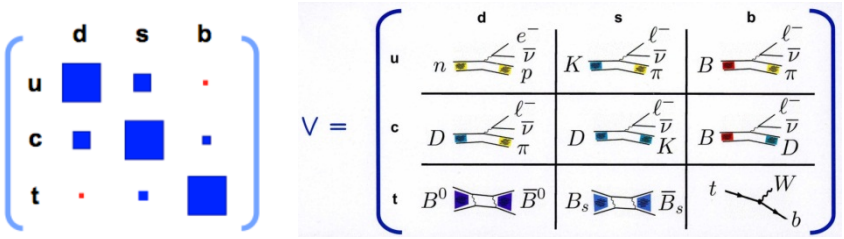

(a) (b)

Figure 1: (a): The magnitude of the CKM elements (b): Methods of experimental extraction of the CKM elements

2.3 Unitarity triangles

A unitarity triangle is a graphic representation of the CKM matrix parameters. from the unitarity of the CKM matrix: $V^+_{CKM}.V_{CKM} = V_{CKM}V^+_{CKM} = 1$; $\Sigma V^*_{ij}V_{ik} = \delta_{jk}$; $\Sigma V_{ij}V^*_{kj} = \delta_{ik}$.
One can deduce 6 non diagonal relations ($\delta_{jk} = \delta_{ij} = 0$) between the matrix's elements

$$V^*_{ud}V_{us} + V^*_{cd}V_{cs} + V^*_{td}V_{ts} = 0 \tag{4}$$

$$V^*_{us}V_{ub} + V^*_{cs}V_{cb} + V^*_{ts}V_{tb} = 0 \tag{5}$$

$$V^*_{ub}V_{ud} + V^*_{cb}V_{cd} + V^*_{tb}V_{td} = 0 \tag{6}$$

$$V^*_{ud}V_{cd} + V^*_{us}V_{cs} + V^*_{ub}V_{cb} = 0 \tag{7}$$

$$V^*_{ud}V_{td} + V^*_{us}V_{ts} + V^*_{ub}V_{tb} = 0 \tag{8}$$

$$V^*_{cd}V_{td} + V^*_{cs}V_{ts} + V^*_{cb}V_{tb} = 0 \tag{9}$$

Every non diagonal relation is represented graphically by a triangle, three of them are shown in Figure 2.

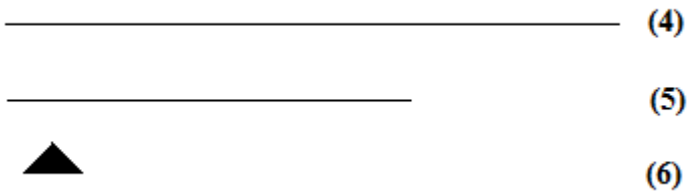

Figure 2: Three of the unitarity triangles

Four of the triangles (4, 5, 7, 9) have two sides much longer than the third side resulting with small angle that could be very difficult to measure. Our interest lies in the two triangles representing the relations 6 and 8. They have three sides with the same order of magnitude in lengths $O(\lambda^3)$. Out of these two triangles, 6 is the most commonly used. Dividing the relation 6 by $V_{cb}^* V_{cd}$ one obtains the re-scaled unitarity triangle shown in Figure3. Its apex is given by the point $(\overline{\rho}, \overline{\eta})$ where $\overline{\rho} = \rho(1 + \frac{\lambda^2}{2})$, $\overline{\eta} = \eta(1 + \frac{\lambda^2}{2})$.
α, β, γ often referred to as ϕ_1, ϕ_2, ϕ_3 are the angles of the unitarity triangle. They can be expressed in terms of the CKM elements:

$$\alpha = arg(-\frac{V_{tb}^* V_{td}}{V_{ub}^* V_{ud}}) \tag{10}$$

$$\beta = arg(-\frac{V_{cb}^* V_{cd}}{V_{tb}^* V_{td}}) \tag{11}$$

$$\gamma = arg(-\frac{V_{ub}^* V_{ud}}{V_{cb}^* V_{cd}}) \tag{12}$$

These angles are related to CP violating symmetries in B decays. If there is no CP violation, all the elements of the CKM matrix are real and the triangle will collapse to a straight line. Thus, measuring those three angles could give us an insight into the degree of CP violation in B system.

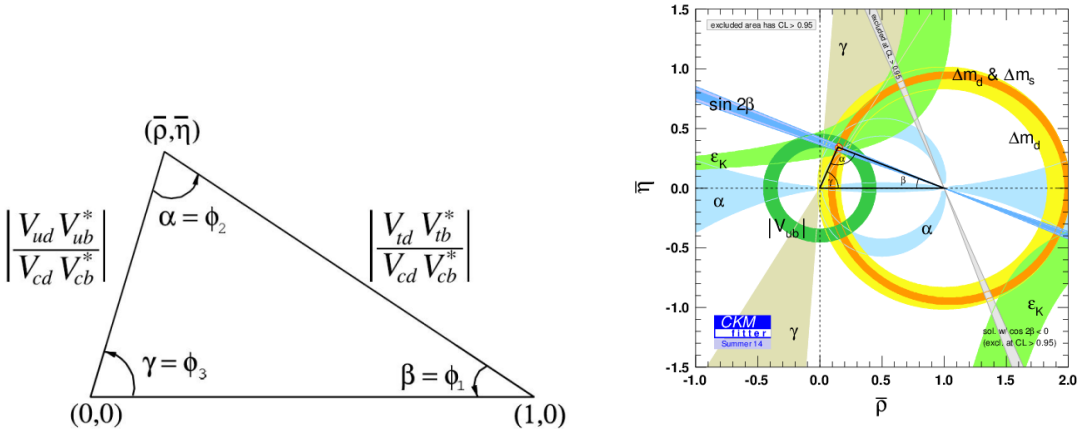

Figure 3: The unitarity triangle

From equation 10 and 11, one can deduce:
$\beta = \pi + arg(V_{cb}^* V_{cd}) - arg(V_{tb}^* V_{td}) = 2\pi - arg(V_{td})$ where V_{cd} is negative and real.
V_{cb}^* and V_{tb}^* are positive and real.
$\beta = -arg(V_{td})$; $V_{td} = |V_{td}|e^{-i\beta}$
$\gamma = \pi + arg(V_{ub}^* V_{ud}) - arg(V_{cb}^* V_{cd}) = arg(V_{ub}^*) = -arg(V_{ub})$
$V_{ub} = |V_{ub}|e^{-i\gamma}$
Hence, the CKM matrix could be introduced as follow:

$$V = \begin{pmatrix} |V_{ud}| & |V_{us}| & |V_{ub}|e^{-i\gamma} \\ |V_{cd}| & |V_{cs}| & |V_{cb}| \\ |V_{td}|e^{-i\beta} & |V_{ts}| & |V_{tb}| \end{pmatrix} + O(\lambda^4)$$

2.4 The CKM angle γ

This angle is the least known angle of the CKM triangle. It can be measured through tree level processes and Loop level processes. The latter could be sensitive to physics beyond the SM ; new physics could appear in loops as virtual particles. Nonetheless, this is not the case for tree level processes which are unaffected by the new physics. γ in tree level processes (γ_{SM})can be used as a SM reference point ("Standard candle") for searches of NP phenomena. The more accurate is the measurement of γ , the more stable the SM reference for the consistency tests of the global CKM fit [8]. One of the current challenges faced by the LHCb is the limitations on the measurement of γ due to statistics uncertainties. However with the 2011 and 2012 Data, LHCb is already better than the previous B-factories Babar and Belle. The constraints on γ from different set of measurements on $D^{(*)}K^{(*)}$ decays [9] are shown in table 1.

Table 1: Constrains on the CKM angle γ

$\gamma(Babar)$	$(70 \pm 18)^0$
$\gamma(Belle)$	$(73^{+13}_{-15})^0$
$\gamma(LHCb)$	$(74.6^{+8.4}_{-9.2})^0$
$\gamma(combined)$	$(73.2^{+6.3}_{-7.0})^0$

2.5 γ extracting methods

Many methods have been proposed to extract γ in B-meson decays ($B^\pm \to D^{0(*)}K^{\pm(*)}$). The most three well known methods are: GLW (Gonau, London and Wyler)Method [10], ADS (Atwood, Dunietz, Soni)Method [11] and GSSZ (Giri, Grossman, Soffer and Zupan)[12] Method. Every method is characterized by different final states of D decays. But, they are all based on interference between the amplitudes of two tree level processes $B^\pm \to D^0K^{*\pm}$ and $B^\pm \to \overline{D^0}K^{*\pm}$ in which the D^0 and $\overline{D^0}$ decay into the same final state.
The Feynman diagrams of B^- decays are shown in Figure 4. The diagram on the left with the $b \to c\bar{u}s$ transition color favored and the one on the right with the $b \to u\bar{c}s$ transition is color suppressed.

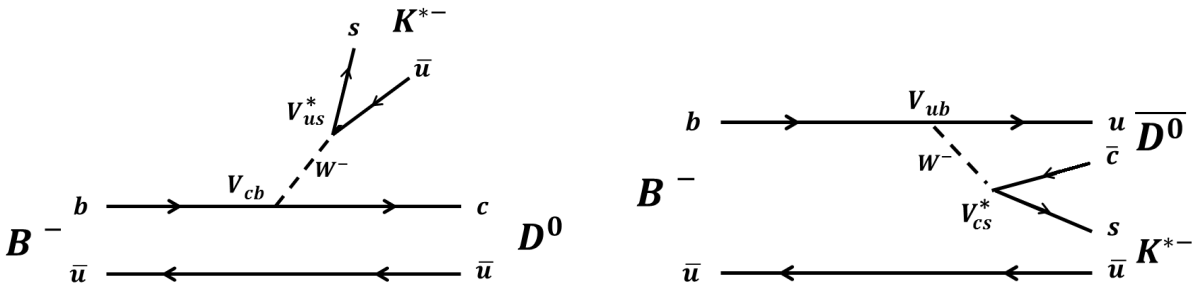

Figure 4: Tree-level Feynman diagrams of the B^- decays.On the left, color favored decay and on the right color suppressed decay

The angle γ is related to the phase of the CKM matrix element V_{ub} through $V_{ub} = |V_{ub}|e^{-i\gamma}$. Hence, the amplitudes of the two processes are:
$A(B^- \to D^0K^{*-}) = |A_c|e^{i\Delta_c}$;$A(B^- \to \overline{D^0}K^{*-}) = |A_u|e^{i\Delta_u}e^{-i\gamma}$
Where Δ_c and Δ_u are the strong phases of the decay (unchanged under CP transformation) and A_q is the amplitude of the transition $b \to q$ with q = u or c. One can usually define r_B the ratio of the amplitudes of the two processes: $r_B = |\frac{A(B^- \to \overline{D^0}K^{*-})}{A(B^- \to D^0K^{*-})}| = |\frac{A(B^+ \to D^0K^{*+})}{A(B^+ \to \overline{D^0}K^{*+})}| = |\frac{A_u}{A_c}|$
r_B is a very important parameter for the γ measurements, the larger it is the higher the sensitivity is to γ and V_{ub}. The current constraint on r_B from existing measurements by BaBar and Belle and averaged by CKMfitter is: $r_B(DK^*) = 0.137^{+0.051}_{-0.047}$ [9]
The next two sections will cover the two methods GLW and ADS:

2.5.1 The GLW Method

The First method for measuring γ using charged $B^{\pm}$ decays, where the D-meson(D^0 or $\overline{D^0}$) decays into CP even eignestates (K^+K^-, $\pi^+\pi^-$) or CP odd eigenstates ($K^0_s\pi^0$,$K^0_s\omega$...)
The CP eigenstate $D^0_{\pm}$ of the neutral D meson is given by : $|D^0_{\pm}\rangle = \frac{1}{\sqrt{2}}(|D^0\rangle \pm |\overline{D^0}\rangle)$
In this case one can deduce the decay amplitudes of $B^{\pm}$:
$A(B^- \to D^0_{\pm}K^{*-}) = \frac{1}{\sqrt{2}}(A(B^- \to D^0K^{*-}) \pm A(B^- \to \overline{D^0}K^{*-}))$
$A(B^+ \to D^0_{\pm}K^{*+}) = \frac{1}{\sqrt{2}}(A(B^+ \to D^0K^{*+}) \pm A(B^+ \to \overline{D^0}K^{*+}))$
In order to determine γ, first of all four CP asymmetries should be introduced:

$$R_{CP_{\pm}} = 2\frac{\Gamma(B^- \to D^0_{\pm}K^{*-}) + \Gamma(B^+ \to D^0_{\pm}K^{*+})}{\Gamma(B^- \to D^0K^{*-}) + \Gamma(B^+ \to \overline{D^0}K^{*+})} = 1 + r_B^2 \pm 2r_B cos\delta_B cos\gamma \tag{13}$$

$$A_{CP_{\pm}} = \frac{\Gamma(B^- \to D^0_{\pm}K^{*-}) - \Gamma(B^+ \to D^0_{\pm}K^{*+})}{\Gamma(B^- \to D^0_{\pm}K^{*-}) + \Gamma(B^+ \to D^0_{\pm}K^{*+})} = \pm\frac{2r_B sin(\delta_B)sin(\gamma)}{R_{CP_{\pm}}} \tag{14}$$

where $\delta_B = \Delta_u - \Delta_c$ is the strong phase difference between the two B decays.
The proof of the previous two equations is given in Appendix A.
As one can see, there exists three unknown variables(δ_B, r_B, γ)and four quantities that could be measured experimentally. Therefore γ could be finally determined with ambiguities.
For this work the CP-odd eigenstates were not included. They are very difficult to study in LHCb due to the limited efficiency in reconstructing and selecting K_s and π^0.

2.5.2 The ADS Method

For this method, the D-meson decays to a non-CP eigenstate ($f = K^+\pi^-, K^-\pi^+$...). For this section the final state f was chosen to be $K^+\pi^-$. This method is based on the interference between the cabibbo (color) favored B decay(seen in Figure 4)followed by the Doubly Cabibbo suppressed D^0decay($D^0 \to K^+\pi^-$)and the cabibbo (color) suppressed B decay followed by the Cabibbo favored $\overline{D^0}$ decay($\overline{D^0} \to K^+\pi^-$). (see Figure 5)

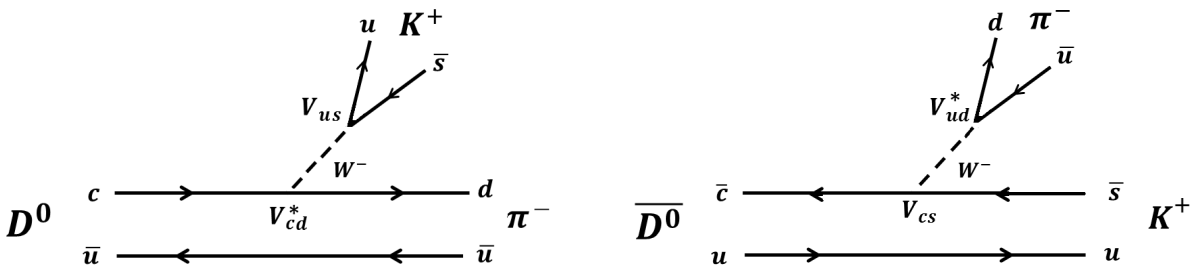

Figure 5: Tree-level Feynman diagrams of the D-meson decays. On the left, doubly Cabibbo suppressed decay and on the right Cabibbo favored decay.

One can define r_D the ratio of the amplitude of the Doubly-Cabibbo suppressed D^0 decay to that of the cabibbo favored D^0decay.
$r_D = |\frac{A(D^0 \to K^+\pi-)}{A(D^0 \to K^-\pi+)} = |\frac{A_{K^+\pi^-}}{A_{K^-\pi^+}}| = \frac{|A_f|}{|A_{\overline{f}}|}$.
r_D is measured in charmed mesons decays $r_D^2 = (0.349 \pm 0.004) \times 10^{-2}$ [13]. Experimentally, two CP asymmetries are measured. They are defined by:(the full proof is given in Appendix A)

$$R_{ADS} = \frac{\Gamma(B^- \to D[\to f]K^{*-}) + \Gamma(B^+ \to D[\to \overline{f}]K^{*+})}{\Gamma(B^- \to D[\to \overline{f}]K^{*-}) + \Gamma(B^+ \to D[\to f]K^{*+})} = r_B^2 + r_D^2 + 2r_B r_D cos(\delta_B + \delta_D)cos(\gamma) \tag{15}$$

$$A_{ADS} = \frac{\Gamma(B^- \to D[\to f]K^{*-}) - \Gamma(B^+ \to D[\to \overline{f}]K^{*+})}{\Gamma(B^- \to D[\to f]K^{*-}) + \Gamma(B^+ \to D[\to \overline{f}]K^{*+})} = \frac{2r_B r_D sin(\delta_B + \delta_D)sin(\gamma)}{R_{ADS}} \tag{16}$$

where $\delta_D = \Delta_{\overline{f}} - \Delta_f$ is the strong phase difference between the two D^0 decay amplitudes. This phase is measured in charmed D decays $\delta_D = (7.3^{+9.8}_{-11.3})^0$ [13]. Once again as a result of the experimental measuring of both A_{ADS} and R_{ADS}, the value of γ is extracted.

3 The LHCb detector

The large Hadron collider beauty (LHCb) experiment is one of the four main experiments at the Large Hadron Collider LHC at CERN [14]. It's dedicated for the precision measurements of CP violation and rare decays of beauty and charm hadrons. Contrary to ATLAS and CMS which are built as 4π detectors, LHCb is a single-arm spectrometer with a forward angular coverage from approximately 15 mrad to 250 mrad in vertical (horizontal) plane. This geometry was chosen because b-hadrons are produced in pairs in the same forward or backward cone at high energies. The LHCb detector consists of different layers ; collectively these sub-detectors gather information about the energy, momentum and identity of each particle. Its first sub detector VELO is built around the proton-proton collision point, with the others following one behind the other over a length of 20 meters.

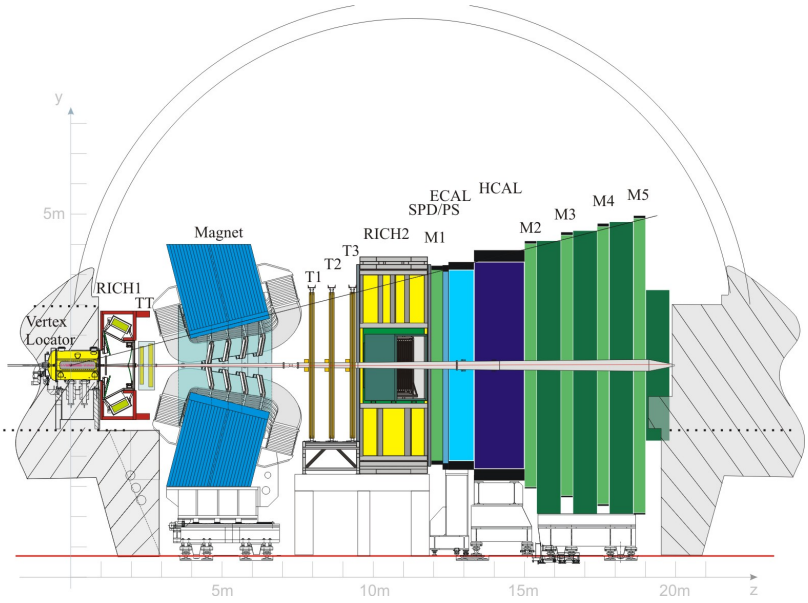

Figure 6: The LHCb detector with its main sub-detectors

The next subsections will describe the main aspects of the LHCb sub-detectors related to this particular study:

3.1 The Tracking system

The Tracking System is dedicated to the reconstruction of particle tracks and measure their momenta. The tracking system is composed by the VErtex LOcator (VELO)3.1.1, the LHCb magnet3.1.2 and the four tracking stations 3.1.3.

3.1.1 The VErtex Locator (VELO)

The main job of VELO is to measure precisely the vertices close to the interaction point not to mention separate the B-mesons from other particles created early on in the detector. B-mesons fly for a few centimeters before decaying so they are never measured directly. However, their existence could be deduced using the distance of separation between the primary vertex (pp interaction point) and the B-meson decay vertex measured by VELO. Hence, the position of B particles can be located to within 10^{-3} mm. This sub-detector consists of two rows of half-disc shape silicon sensors (25 stations in total), providing a measurement for the ϕ and r coordinates. VELO is shown in Figure7

3.1.2 The magnet

LHCb uses an non supra-conducting dipole magnet consisting of two identical coils and weighing 1.600 Tons. It provides an integrated magnetic field of 4 Tm used to bend the trajectory of charged particles. By examining the curvature of the path, it's possible to calculate the momentum of a charged particle given by $P(Gev/c) = 0.3B(T)R(m)$ where B is the magnetic field and R is the radius of the curvature. Thus, its identity could be established.

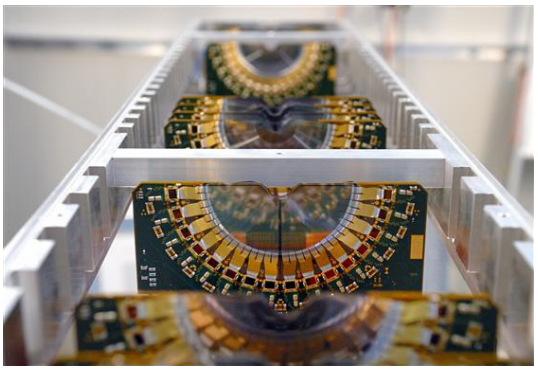

Figure 7: the VErtex Locator VELO

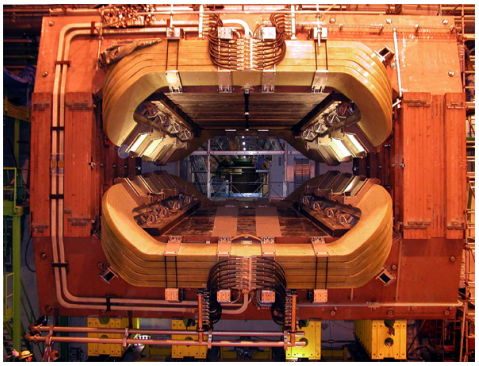

Figure 8: The LHCb magnet

3.1.3 The tracking stations

TT (The silicon Tracker Turicensis) is located $2.5m$ downstream of the proton-proton interaction point allowing the reconstruction of the vertices of long lived particles decaying outside the volume of VELO(e.g Ks). TT stations, $1.5m$ wide and $1.3m$ high, surrounds the beam pipe and consists of layers of silicon micro-strip sensor (IT). The other three stations T1 T2 T3, $6m$ wide and $4.9m$ high, are located downstream of the magnet and made of gas filled straw-tube drift chamber(OT)expect for a small area around the beam pipe where silicon micro-strip detectors (IT) are used. Whenever a particle passes through the gas tubes of OT, it ionizes gas molecules liberating electrons. The drift time is measured with respect to the LHC radio-frequency clock hence the spatial position of the track is found. When it passes through the silicon tracker, due to the successive collisions with silicon atoms an electric signal is generated indicating the path of the particle. The four tracking stations are shown in Figure 9, where (IT) are represented in purple and (OT) in blue.

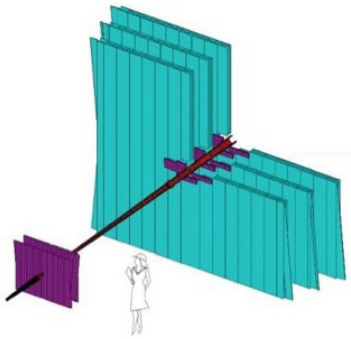

Figure 9: LHCb tracking stations

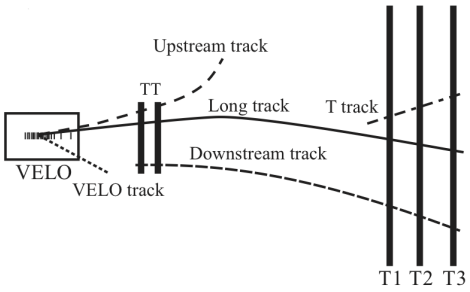

Figure 10: Track types

For $5 < p < 100$ Gev/c a momentum resolution of $\frac{\delta p_T}{p} = 0.5\%$ or better is needed to achieve a good invariant mass resolution at LHCb.

Tracks of the particles are reconstructed using the information coming from the different parts of the tracking system. These tracks could be divided in different categories :Long Tracks, Downstream Tracks, Upstream Tracks, VELO tracks and T tracks.

For the analysis of this internship, two different types of Ks tracks were used. Long K_s tracks "K_sLL" and the Downstream K_s tracks "K_sDD". As one can see in Figure 10, Long Tracks cross the full tracking system from the VELO to the tracking stations. They usually have the best momentum resolution. On the other hand, Downstream Tracks are produced outside the VELO and they leave hits only in TT and T1-T3 stations.

3.2 RICH detectors

The LHCb detector includes two Ring Imaging Cherenkov detectors RICH1 and RICH2. RICH1 with Silica aerogel and C_4F_{10} gas radiators, positioned directly after the vertex detector and before the main tracking system. It is used for particle identification of low momentum tracks. RICH2 with CF_4 gas radiator placed after the tracking stations and in front of the calorimeters it allows the identification of the particle type of high momentum tracks.

This detector depend on the Cherenkov radiation emitted at angle θ_c to the trajectory of a charged particle traveling at a velocity higher than the speed of light in a medium with index $n > 1$. The Cherenkov angle θ_c is given by: $cos(\theta_c) = \frac{c}{nv}$

Knowing θ_c and the momentum p of a particle (measured by the main tracking system), the particle could be identified.The two RICH detectors are responsible for identifying a wide range of charged particles including Pions, Kaons and Protons. (see Figure11)

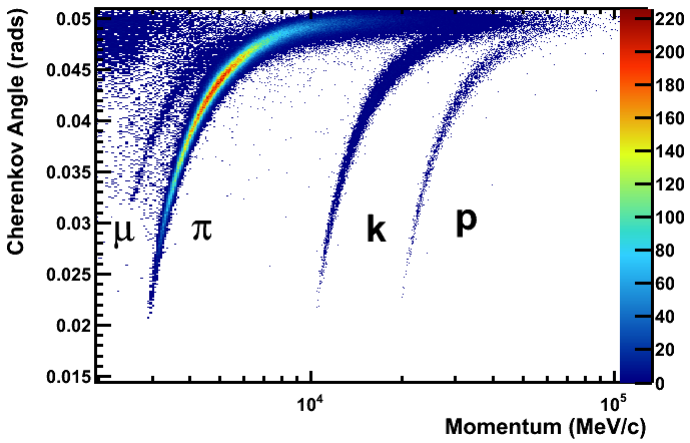

Figure 11: Reconstructed Cherenkov angle as a function of track momentum in the C_4F_{10} radiator.

The other subdetectors (caloremeters and Muon stations) are not relevant for this internship thus they are not described any further.

4 Analysis of the decay channel $B^{\pm} \to D[hh]K^{*\pm}[K_s\pi^{\pm}]$

4.1 Overview

In order to extract the CKM angle γ using the decay channel $B^{\pm} \to D[hh]K^{*\pm}[K_s\pi^{\pm}]$. First of all, one must reject all the background related events through a series of selections on discriminating variables described in details in subsection4.4. Two types of background will be dealt with for this analysis. The first type is the combinatorial background coming from random combinations of tracks having an invariant mass close to that of the particles of the studied decay channel. The second type is known as the physics background arising from partially reconstructed decay channels or from fully reconstructed particles decaying into the same final state of a particle involved in this decay channel. A bottom-up approach will be used for the event selection process where one starts to perform the selection cuts on the discriminating variables of the daughter particle K_s afterwords on K^*'s and D's variables and finally the mother particle B. Once the signal is completely purified, the surviving events will be used either for the GLW or the ADS method. The decay topology is shown in Figure 12. The B-meson will fly in the detector for approximately $1.3cm$ (see Table6) before decaying into a D-meson and a $K^*(890)$. After traversing about $5.6mm$, the D-meson will decay to a CP eigenstate ($\pi^+\pi^-$, K^+K^-) or to a non CP eigenstate $K^{\pm}\pi^{\pm}$. On the other hand, K^* due to its very short lifetime $\tau = 1.3 \times 10^{-23}s$ it will decay instantly into a $K_s\pi$ final state.

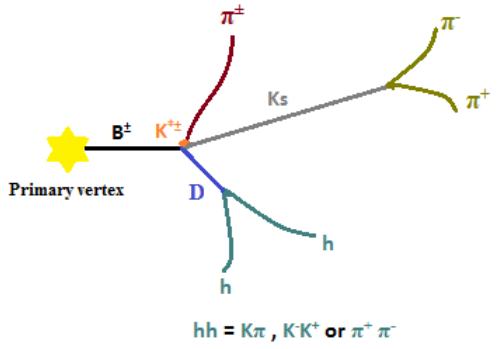

Figure 12: The Topology of the decay

Using the DataSet described in subsection4.2. This decay chain was reconstructed in two categories where two different types of K_s's tracks were used. When analyzing the decay channel of the category where K_sLL (K_sDD) was used it will be referred to in the following sections as simply "LL" ("DD").

4.2 Used DataSet

For this analysis two different data samples were used. The first one consists of a Monte Carlo simulation sample also known as "the truth" that was generated to mimic the experimental conditions and performance of the LHCb detector. The proton proton collisions and resulting decays of generated particles(e.g B-mesons), were simulated by the EvtGen package [15]. GEANT 4 [16] was used to simulate the passage and interaction of the decay products with the LHCb detector. The second sample used is the data collected by the LHCb detector during the LHC run in 2011(2012) with a center of mass energy $\sqrt{s} = 7(8)TeV$ and integrated luminosity $L_{2011}(L_{2012})$ of $1.04(2.03)fb^{-1}$. The data has been reconstructed with the LHCb event reconstruction application Brunel[17] and stripped using the DaVinci package[18]. Then, the events reconstructed as the decay chain that we are interested in shown in Figure12 are preselected and stored in many RooTtree files using the massive parallel processing of data through the GRID facility. The present work of this internship will start from the preselected and stripped data.

Renormalization: A comparison between these two data samples should take place in the event selection process of this analysis. But since they do not fit the same Luminosity it's essential to renormalize the Monte Carlo sample with respect to the LHCb data sample. One can proceed first by the determination of the expected number of $B^{\pm}$ mesons produced in the acceptance of LHCb in 2011 and 2012 given by the following relation:

$$N_B = L\sigma = L_{2011}\sigma_{2011} + L_{2012}\sigma_{2012} \tag{17}$$

where σ_{2011} is the cross section of the B-mesons production in the acceptance of LHCb in 2011 at 7Tev [19]:
$\sigma_{2011} = 38.9 \pm 0.3(stat.) \pm 2.5(syst.) \pm 1.3(norm.)\mu b$
The cross section σ_{2012} at 8Tev is approximately 10% bigger than that of 2011 : $\sigma_{2012} = 1.1\sigma_{2011}$. Using equation 17, One gets $N_B = 1.27 \times 10^9$. In order to determine the number of B mesons decaying into the particular decay channel studied for this analysis, the relation 17 will be multiplied by the branching ratio Br:
$N_{LHCB_{data}} = Br(B \to D[hh]K^*[K_s[2\pi]\pi]).N_B = 6597962$
On the other hand for the Monte Carlo simulation sample, the number of simulated events of the decay channel $B \to D[hh]K^*[K_s\pi]$ in the LHCb detector acceptance 2011 and 2012 is $N_{MCS} = 603038$.
From these two results the renormalization factor is deduced $\dfrac{N_{LHCBdata}}{N_{MCS}} = 10.94$

4.3 Mass sidebands

To achieve excellent control over the background noise events for this decay channel. The zones where the combinatorial background noise events are expected to dominate the signal and vise versa should be defined using the masses of the main particles of this decay B, D, Ks. The signal shape of the masses is described by the Gaussian distribution (see Figure 4.3) thus, the mass resolutions σ_B ,σ_D and σ_{Ks} are provided from the Gaussian fit of the MC masses distributions and their values are summarized in table2.

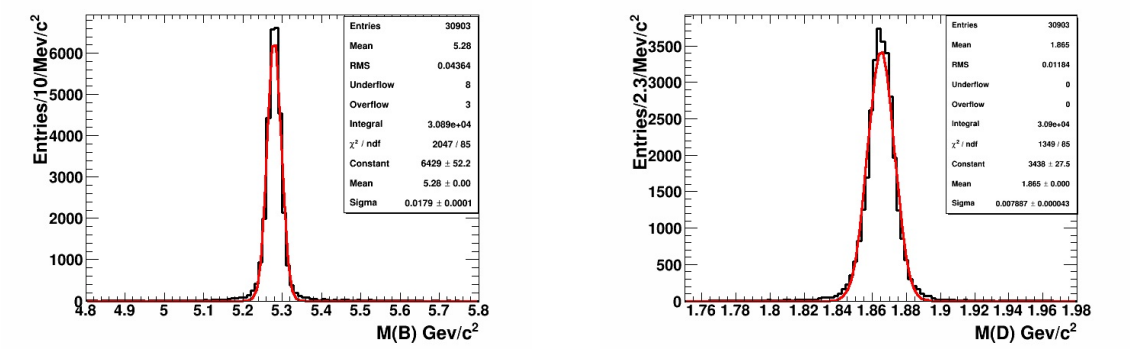

Figure 13: Fitted MC mass distributions of B and D

Table 2: Mass resolution of B, D and K_s

Particle	Mass resolution $\sigma(Mev/c^2)$
B	17.78 ± 0.23
D	8.029 ± 0.099
Ks LL	3.686 ± 0.048
Ks DD	6.6188 ± 0.05

Figures14 illustrates the different types of events dealt with for the DD analysis. Three main zones could be defined:

- The Red Zone where one expects to see the signal. The events of this zone have the reconstructed invariant masses $M(B)(M(D))$ within the 3 standard deviations $\sigma_B(\sigma_D)$ of the PDG mass value $M(B)_{PDG}$ $(M(D)_{PDG})$.

- The Blue Zone(D and B side-band) where $M(B)$ and $M(D)$ are above 5σ of the M_{PDG}. Only combinatorial background noise events for both B and D are expected to appear in this zone.

- The Green Zone (B upper side-band) where one expects to see combinatorial background events for $B(M(B) > M(B)_{PDG}+5\sigma_B)$ and real signal events for D $(M(D) \in (M(D)_{PDG} \pm 3\sigma_D))$.

For the LL analysis, Figure15 shows the different side-bands, this time the same constrains were used on $M(KsLL)$ instead of $M(D)$.

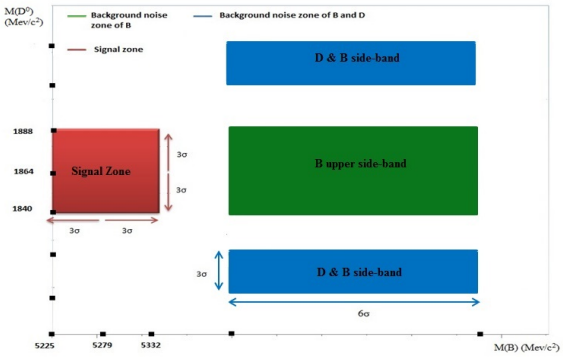

Figure 14: Mass side-bands for DD

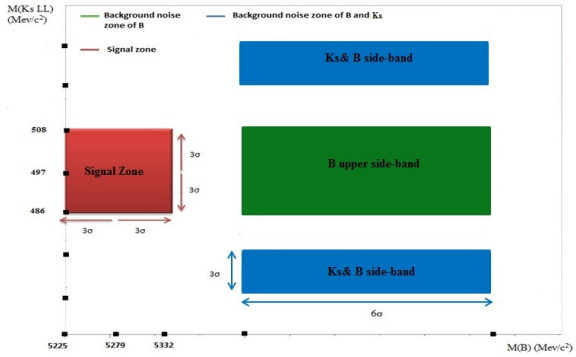

Figure 15: Mass side-bands for LL

The strategy is to use for the event selection process the BLUE and GREEN sidebands with the LHCb data to define the background like discriminating variables, while the signal like variables are obtained with the Monte Carlo simulation in the RED zone. More details will be provided in subsection 4.5.

4.4 Discriminating variables

Discriminating variables are either topological or kinematic variables used to separate the background related events from the signal related events. In total 14 discriminating variables were

exploited for this decay channel. These variables will prove to be useful not only for the rejection of combinatorial background but also for physics background. A brief description will be provided for all the variables.

Discriminating variables of K_sDD and K_sLL

- $\frac{\Delta Z(K_s - B)}{\sqrt{\sigma^2_{K_s} - \sigma^2_B}}$:
  The separation between K_s and B vertices in the Z-direction over the vertex errors. This variable could be suitable to remove random $\pi^+\pi^-$ combinations directly originated from the primary vertex instead of the decay of K_s. For instance, A selection cut on this variable could greatly reduce the background related to the decay channel $B \to D\pi^+\pi^-\pi^+$ which has a branching ratio 10 times bigger than that of $B \to DK^*$. Since K_s is a decay product of B, its Z-position should be well downstream the B vertex therefore its value for a signal event could never be negative. If one finds the contrary, it can be deduced that it's a background event.

- $\chi 2$ FD K_s:
  The flight distance of a particle is the distance between the originating point(primary, secondary vertex) of the particle in question and its decay vertex. This variable can determine whether the value of the flight distance of K_s for the observed events are significantly different from the expected values.

- $Log(DIRA_{K_s})$:
  $DIRA$ is the cosine of the angle between the momentum vector of K_s and the flight distance vector from the primary vertex to K_s's decay vertex. For a two body decay, these two vectors should be collinear. Hence, the value of $DIRA$ for a signal event should not be very far from 1.(See Figure 16). If the particle is in fact decaying to a 3 or more tracks in which not all of them were reconstructed or if the tracks of the reconstructed particle were ill chosen, the two vectors will not be collinear.

Discriminating variables of K^*

- $cos(\theta_{Helicity_{Ks}})$
  The helicity angle $\theta_{helicity_{Ks}}$ is defined as the angle between K^*(vector) and K_s(pseudo scalar), measured in the rest frame of K^*.
  The decay $K^* \to K_s\pi$ is of the type : V $\to$ S + S .
  Which means that for signal events, this decay channel produces an helicity angle distribution proportional to cos^2 and it's supposed to be flat for background events.

- Particle Identification PID by the RICH subdetector.
  As mentioned in subsection 3.2, the RICH sub-detectors are mainly dedicated to discriminate between charged particles like Kaons and pions. For the decay of K^*, it's crucial to not misidentify the pion as kaon or a proton. For Instance, a huge background contribution will originate from the decay channel $B^{\pm} \to DK^{\pm}K_s$ if the Pion (daughter particle of K^*) in the decay channel we are interested in is misidentified as a Kaon. For this reason, this variable was introduced.It's defined as:
  $PID_{\pi} = probNN\pi \times (1 - probNNK) \times (1 - probNNp)$
  Where $probNNX$ is the probability for a particle $X = p, K, \pi$ to be identified as a Proton, Kaon or a Pion.

Discriminating variables of D

- $P_T(K^*)\&P_T(D)$
  B-mesons are produced in the same forward cone in high energies and as a result of their large mass, B-meson decays tend to produce daughter particles (in this case D and K^*) with high transverse momenta (P_T). Using the transverse momenta of K^* and D one can easily tell the difference between background and signal.

- $Log(DIRA_D)$:
  The same variable used for K_s, the only difference here is that $DIRA_D$ is the cosine of the angle between the momentum vector of D and the flight distance vector from the primary vertex to D's decay vertex.

- $\dfrac{\Delta Z(D-B)}{\sqrt{\sigma_D^2 - \sigma_B^2}}$
  The separation between K_s and B vertices in the Z-direction over the vertices errors. This variable helps to reject background contributions from charmless B decays for example :
  $B^- \to K^-K^+K^{*-}$ with a branching ratio 17 times bigger than that of $B^- \to [K^-K^+]_D K^{*-}$.
  $B^- \to \pi^-\pi^+K^{*-}$ with a branching ratio 101 times bigger than that of $B^- \to [\pi^-\pi^+]_D K^{*-}$.

- $DoCa$:
  $DoCa$ is the distance of the closest approach of the particle D to the pp interaction point.

Discriminating variables of B

- $\chi 2$ of IP: The impact parameter (IP) is the shortest transverse distance between a particle trajectory and the primary vertex (see Figure17). IP is expected to be very small for particles originating from the primary vertex (e.g B-mesons). For The daugter particles (e.g B-daugter particles: D, K^*) emerging from secondary vertices, IP is expected to be bigger.

- $cos(\theta_{Helicity_D})$ The helicity angle $\theta_{helicity_D}$ is defined here as the angle between the momentum of B(Pseudosclar) and the momentum of D (Pseudoscalar), measured in the rest frame of B. The decay $B \to K^*D$ is of the type : S $\to$ V + S. The signal events of this decay channel produces an helicity angle distribution proportional to sin^2.
- Two other variables already described for different particles were also used $\chi 2$ FD of B & $Log(DIRA_B)$

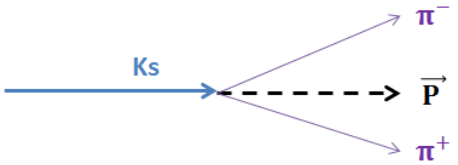

Figure 16: Ks two body decay
Where $DIRA = 1$

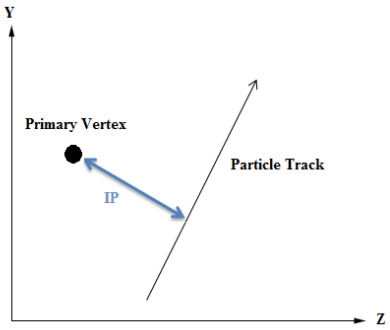

Figure 17: IP of a track with respect to the primary vertex

Invariant mass window : In order to eliminate the remaining background events after the selection on the different discriminating variables. A mass cut will be applied on the invariant mass of the particle in question. For instance, after the selections on K_s's 3 discriminating variables all the events which do not respect this condition $|M(Ks)_{PDG} - M(Ks)| > 3\sigma_{Ks}$ will be rejected. The same condition will be also applied for the invariant mass of D. As for K^* which has a wide natural width, a mass cut will be performed at $\pm$100 Mev around the peak of the mass distribution. All the values of these cuts are summarized in table4.

4.5 Event selection optimization

The aim of this part of the analysis is finding the most efficient selection on the discriminating variables in order to allow the best separation between background noise and signal events. This could be achieved by maximizing the significance $Q = \frac{S}{\sqrt{S+B}}$, where S is the number of signal events and B is the number of background-noise events. Events distribution for each variable mentioned in subsection 4.4 were compared for two different data samples: The MCS sample in the Red zone "the signal sample" and the LHCb data in the blue zone or in the green zone "the background noise sample". The significance is deduced and selection cuts are applied.
Few examples of the selection optimization are illustrated in Figures 18,20,22 additional examples are shown in the Appendix B. The selection cut values are given in table 5.

$\Delta z(KsDD - B)$/vertex errors distributions are shown in Figure 18, as mentioned earlier the background noise distribution shown in blue takes negative values while the signal sample shown in red starts from zero. The significance (Figure 19) is maximized at a value equal to 7 hence all the events below the maximum are rejected.

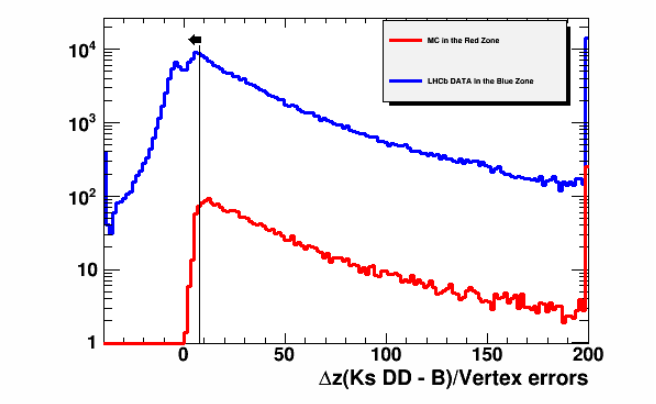

Figure 18: Δz(Ks DD -B)/vertex errors

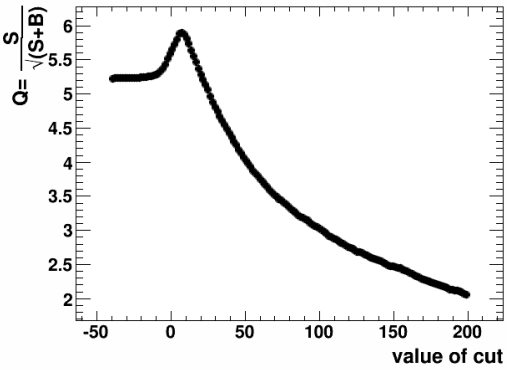

Figure 19: The significance Q

The distributions of χ^2 of the flight distance of D are shown in Fig 20. The significance (Figure 21) in this case is maximized at a value equal to 500 all the events below this value are rejected.

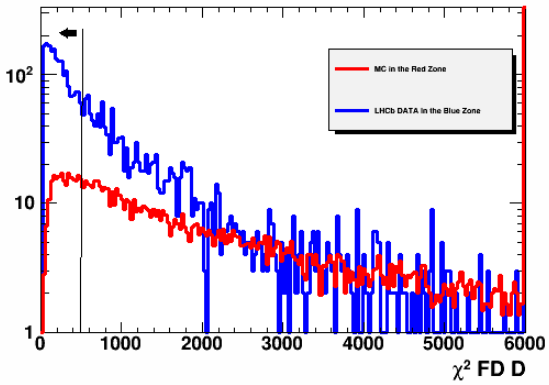

Figure 20: χ^2 D FD distributions

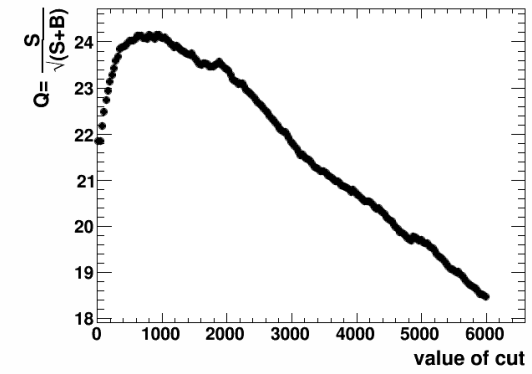

Figure 21: The significance Q

For certain discriminating variables, the significance could not be maximized. Hence, the value of the selection cut was chosen to keep the signal efficiency almost intact while decreasing the efficiency of the background noise as much as possible. This is the case of $Log(DIRA_B)$ shown in Figure 22. The selection cut was chosen to be -14. This choice preserved about 90% of the signal efficiency and only 25% of the background efficiency(Figure 23).

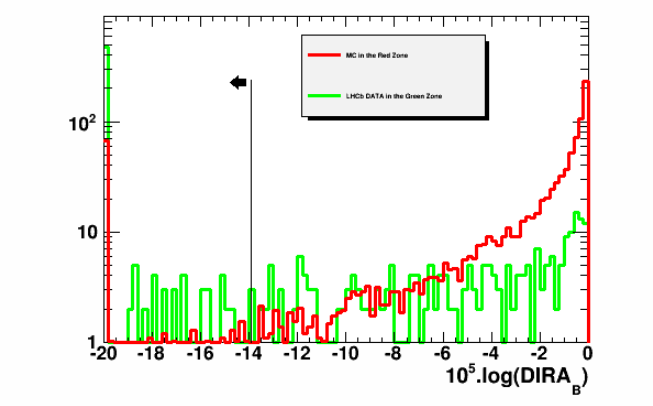

Figure 22: $log(DIRA_B)$ distributions

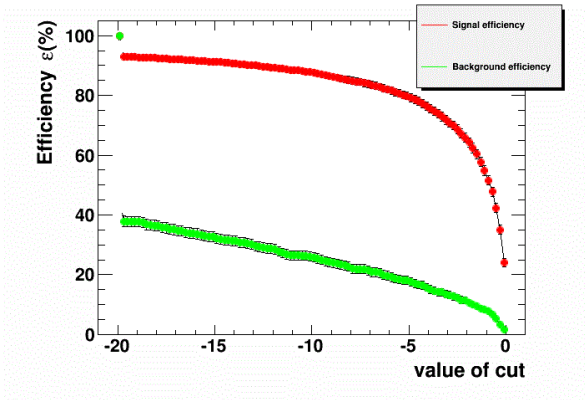

Figure 23: Signal and Background efficiency

5 Results

5.1 After event selection : The invariant mass distributions

In this subsection, the reconstructed invariant mass distributions of the particles (K_s, K^*, D, B) will be shown before and after the selection process for the DD analysis.
The mass distribution of K_sDD is shown in Figure 24. After the selection on the 3 discriminating variables of K_s, one can see clearly that the level of the background has decreased and the mass distribution after the selection and the mass cut (in green) took more of a Gaussian shape.

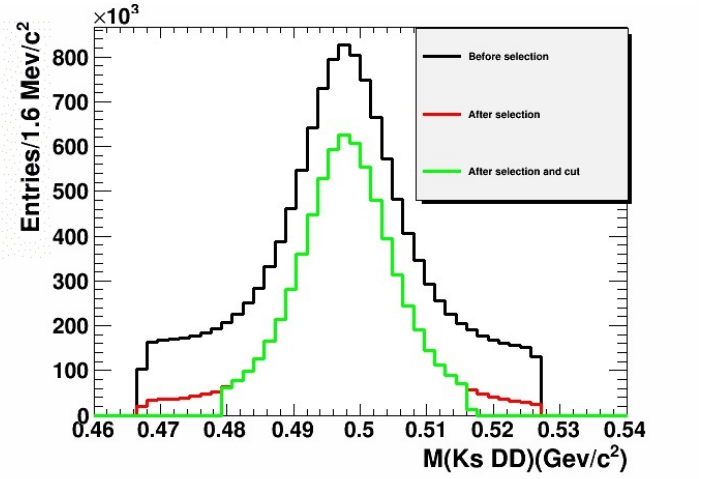

Figure 24: The reconstructed invariant mass M(K_{DD})

Initially the signal of $K^*(890)$ was drowned by the background (Figure 25). One could barely see its peaking structure rising above the background at approximately $0.89 Gev/c^2$. The mass distribution of $K^*(890)$ features also two other peaks at approximately 1.6 and $1.9 Gev/c^2$. They

are associated to the physics background, the first one is $K^*(1680)$ and the second one is $D^{\pm}$. They both decay into $K_s\pi^{\pm}$ the same final state of $K^*(890)$. These two peaks along with the combinatorial background noise were successfully subtracted after the selection and the mass cuts.

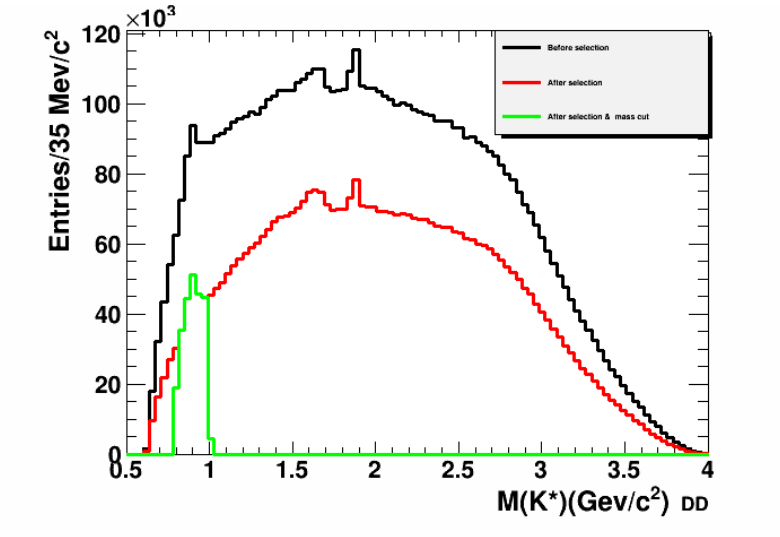

Figure 25: The reconstructed invariant mass M(K^*)

The mass distribution of D is shown in Figure 26. Before the selection (in Black), an enormous amount of combinatorial background specially around the edges dominated the signal. The green distribution (after the selection optimization and the mass cut) shows that the background is barely existent and the signal peak distinctly appear at $M(D) = 1.68 Gev/c^2$.

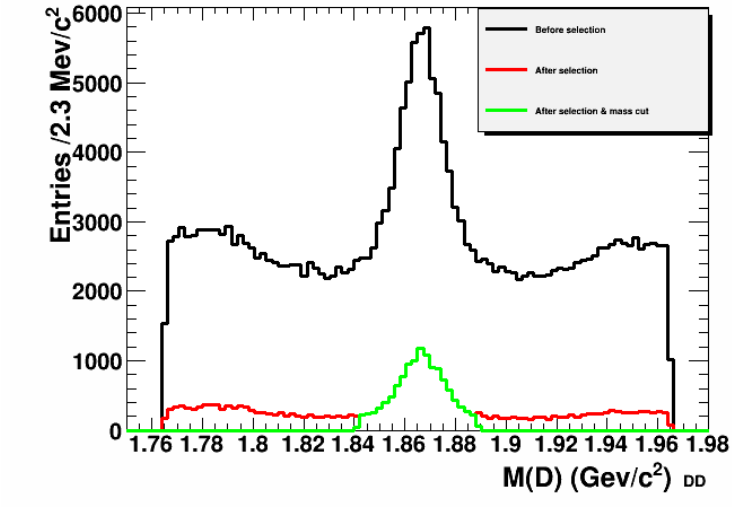

Figure 26: The reconstructed invariant mass M(D)

Finally, with the aim to show the effect and role of every step of the selection process in lowering the background, the mass distribution of the mother particle B was illustrated in Figure 27 after the selection on every one of the 4 discriminating variables of B. The signal peak appears to be around the B mass at $5.29 Gev/c^2$. However, one can observe in Figure 28, additional two smaller peaks. They are caused by the physics background contributions of the partially reconstructed decay channels $B^{\pm} \to D^{*0}[D^0\pi^{\pm}]K^{*\pm}$ where $\pi^{\pm}$ was not reconstructed and $B^0 \to D^{*+}[D^0\pi^+/\gamma]K^{*\pm}$ where π^+/γ was not reconstructed.

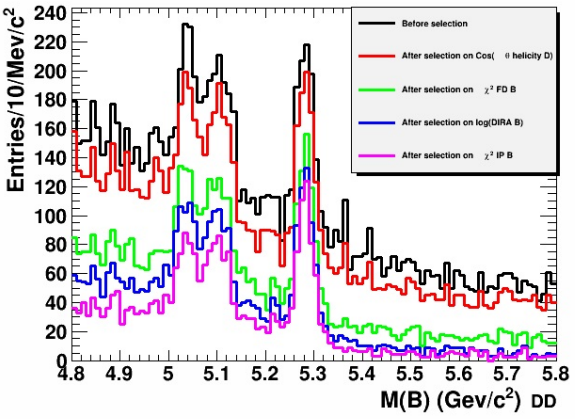

Figure 27: M(B) before and after selection on B's 4 discriminating variables

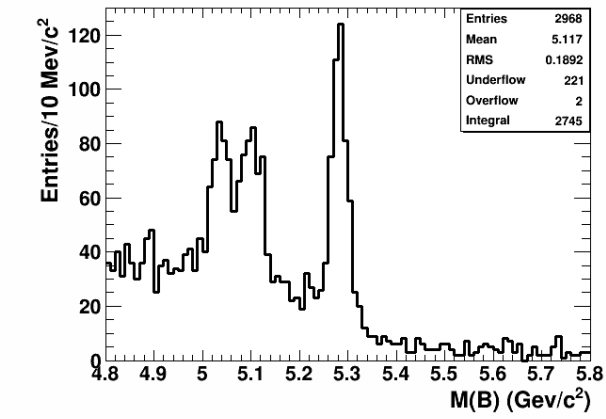

Figure 28: The invariant reconstructed mass M(B) after all the selection cuts

Overall these selection and mass cuts proved to be very useful with a selection efficiency $\epsilon_{selection}$ [1] of 25% for the DD analysis and 18% for the LL analysis.

5.2 CP violation observables

Up to this point, the work was focused on the decay channel $B \to D[hh]K^*[K_s\pi]$ without any assumption what so ever on the charges of the particles nor the identity of D's final state hh. To be able to use this decay channel for the GLW and ADS methods, one must split the surviving events in different categories using ID [20] and PID variables.
The events could be split in 4 different categories:

- $N(B^{\pm}, RS)$: Events of the "Right sign" decay channels where $hh = K\pi$ and the charge of $K^{*\pm}$ is same in sign to $K^{\pm}$.

[1] The selection efficiency is computed using the Monte Carlo simulation: $\epsilon_{selection} = \frac{N_{After}}{N_{Before}}$.
N_{After} is the number of events left after the selection.
N_{Before} is the number of events before the selection.

$B^- \to D[K^-\pi^+]K^{*-}$; $B^+ \to D[K^+\pi^-]K^{*+}$ (The Cabibbo Favored decay events).

- $N(B^\pm, WS)$: Events of the "Wrong sign" decay channels where $hh = K\pi$ and the charge of $K^{*\pm}$ is opposite in sign to $K^\pm$.
  $B^- \to D[K^+\pi^-]K^{*-}$; $B^+ \to D[K^-\pi^+]K^{*+}$ (The Cabibbo Suppressed decay events).

- $N(B^\pm)_{CP_{\pi\pi}}$: Events of the decay channels where D decays into $\pi^+\pi^-$ (CP+ eigenstate)
  $B^- \to D[\pi^+\pi^-]K^{*-}$; $B^+ \to D[\pi^+\pi^-]K^{*+}$.

- $N(B^\pm)_{CP_{KK}}$: Events of the decay channels where D decays into K^+K^- (CP+ eigenstate)
  $B^- \to D[K^+K^-]K^{*-}$; $B^+ \to D[K^+K^-]K^{*+}$.

As already mentioned in subsections 2.5.1 and 2.5.2, the measurement of the CP observables $R_{CP_\pm}$, $A_{CP_\pm}$ (GLW method) and R_{ADS}, A_{ADS} (ADS method) is the first step to determine the angle γ. These observables could be measured experimentally by the following equations:

$$R_{CP_+} = \frac{N(B)_{CP_+}}{N(B, RS)} \times \frac{\epsilon_{RS}}{\epsilon_{CP_+}} \tag{18}$$

$$A_{CP_+} = \frac{N(B^-)_{CP_+} - N(B^+)_{CP_+}}{N(B)_{CP_+}} \tag{19}$$

Where
$N(B)_{CP_+} = N(B^-)_{CP_+} + N(B^+)_{CP_+}$ and CP_+ refers to the KK or $\pi\pi$ final states.
ϵ_{CP_+} and ϵ_{RS} are the correction factors depending on the branching ratio and the selection efficiency. They were introduced to take into consideration the two different D final states used to compute R_{CP_+}.
$\epsilon_{CP_+} = \epsilon_{selectionCP+} \times Br(D \to CP_+)$
$\epsilon_{RS} = \epsilon_{selectionK^-\pi^+} \times Br(D \to K^-\pi^+)$

$$R_{ADS} = \frac{N(B, WS)}{N(B, RS)} \tag{20}$$

$$A_{ADS} = \frac{N(B^-, WS) - N(B^+, WS)}{N(B, WS)} \tag{21}$$

The statistics of both LL and DD were merged together to determine the CP observables with a better precision with the exception of R_{CP_+} which was computed separately for DD and LL.

The numbers of the events that the CP observables depend on could be deduced after a Binned Likelihood fit of the B mass distributions in each case. Four of The fits of M(B) are shown below. The results from the fit and values of the CP observables are summarized in Table 3.

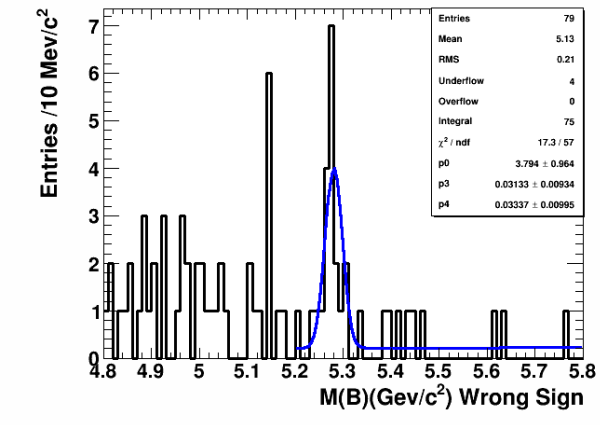

Figure 29: M(B) distribution for the "Wrong Sign" events

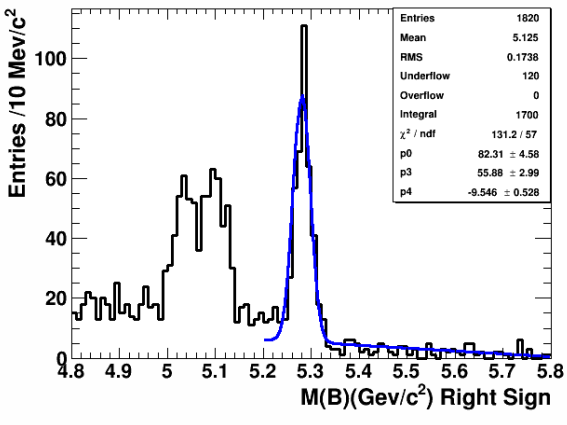

Figure 30: M(B) distribution for the "Right Sign" events

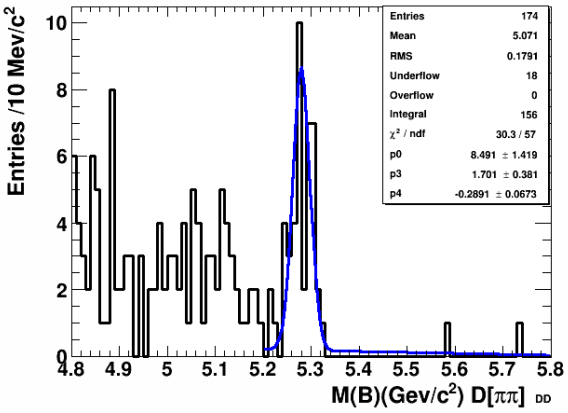

Figure 31: M(B) distribution for $hh = \pi^+\pi^-$ DD

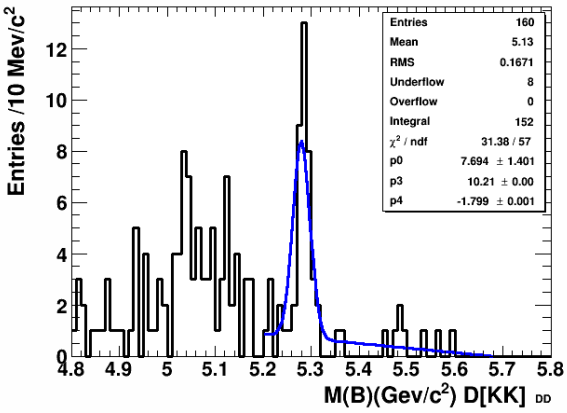

Figure 32: M(B) distribution for $hh = K^+K^-$ DD

The "WRONG SIGN" events signal shown in Figure 29 also known as the "ADS" signal was never observed for this decay channel before, we have statistical significance of 4-standard deviations hence we have an evidence of the WS signal but we needed only 1σ for an observation. As for the "RIGHT SIGN" (Figure 30) and the CP^+ events (Figures 31, 32) we have an observation.

Table 3: The Results from the fit and the CP violation observables for the GLW and the ADS methods

	Number of events [1][2]	$R_{CP_{KK}}$	$R_{CP_{\pi\pi}}$	$A_{CP_{KK}}$	$A_{CP_{\pi\pi}}$
Combined (DD & LL)					
DD		1.24 ± 0.24	3.42 ± 0.64		
$N(B)_{CP_{\pi\pi}}$	38.31 ± 6.722				
$N(B)_{CP_{KK}}$	34.71 ± 6.32				
$N(B)_{RS}$	295.4 ± 18.54				
LL		1.08 ± 0.43	1.49 ± 0.79		
$N(B)_{CP_{\pi\pi}}$	3.87 ± 1.99				
$N(B)_{CP_{KK}}$	8.32 ± 3.16				
$N(B, RS)$	74.44 ± 9.02				
Combined (DD & LL)				0.086 ± 0.164	0.093 ± 0.157
$N(B^+)_{CP_{\pi\pi}}$	19.59 ± 4.54				
$N(B^+)_{CP_{KK}}$	20.08 ± 4.79				
$N(B^-)_{CP_{\pi\pi}}$	23.61 ± 5.01				
$N(B^-)_{CP_{KK}}$	23.86 ± 5.36				
		R_{ADS}		A_{ADS}	
Combined (DD & LL)		0.046 ± 0.012		0.139 ± 0.181	
$N(B^-, WS)$	8.89 ± 3.26				
$N(B^+, WS)$	6.72 ± 2.85				
$N(B, WS)$	17.11 ± 4.34				
$N(B^-, RS)$	194.10 ± 15.069				
$N(B^+, RS)$	177.85 ± 14.39				
$N(B, RS)$	371.37 ± 20.66				

The four values of R_{CP^+} shown above were combined [21], the same for the two values of A_{CP^+}. One can deduce the final results :

$R_{CP^+} = 1.42 \pm 0.19(stat)$

$A_{CP^-} = 0.089 \pm 0.11(stat)$

$R_{ADS} = 0.046 \pm 0.012(stat)$

$A_{ADS} = 0.139 \pm 0.181(stat)$

The same decay channel was studied in 2009 by the Babar collaboration [22]. They got the following results:

$R_{CP^+} = 2.17 \pm 0.35(stat) \pm 0.09(syst)$

$A_{CP^+} = 0.09 \pm 0.13(stat) \pm 0.06(syst)$

$R_{ADS} = 0.066 \pm 0.031(stat) \pm 0.16(syst)$

$A_{ADS} = -0.34 \pm 0.16(stat) \pm 0.010(syst)$

The values of the GLW observables for this study are very compatible with the results found by Babar. As for the ADS signal, they had a statistical significance of 2.1σ so they did not have an observation.

[2]The Number of events in table 3 are determined after a normalization of the fit result:
Number of events $= \frac{\sigma}{Bins_{WIDTH}} \times \sqrt{2\pi} \times P^0_{fit}$

6 Conclusion

The signal events of the decay channel $B \to DK^*$ were selected while the background events were rejected with an efficiency of 25%(18%) for the DD(LL) analysis. The ADS and GLW methods allowed the measurement of the CP violation observables A_{ADS}, R_{ADS}, A_{CP^+}, R_{CP^+}.
During the remaining time of this internship we will attempt to improve if possible the selection efficiency for both DD and LL in order to achieve better results, the systematic errors for the CP observables will be computed. Finally, since the "WRONG SIGN" signal was not observed, at this point it is unlikely to get a precise measurement of the CKM angle γ.

A Appendix - CP violation observables equations

The proof of the CP violation observables equations:

GLW observables

$A(B^- \to D^0 K^{*-}) = |A_c| e^{i\Delta_c}$
$A(B^- \to \overline{D^0} K^{*-}) = |A_u| e^{i\Delta_u - \gamma}$
$A(B^+ \to \overline{D^0} K^{*+}) = |A_c| e^{i\Delta_c}$
$A(B^+ \to D^0 K^{*+}) = |A_u| e^{i(\Delta_u + \gamma)}$
The amplitudes of the two B decays($B^+ \to D^0_\pm K^{*+}; B^- \to D^0_\pm K^{*-}$):

- $A(B^+ \to D^0_\pm K^{*+}) = \frac{1}{\sqrt{2}}(A(B^+ \to D^0 K^{*+}) \pm A(B^+ \to \overline{D^0} K^{*+})$
  $A(B^+ \to D^0_\pm K^{*+}) = \frac{1}{\sqrt{2}}(|A_u| e^{i(\Delta_u + \gamma)} \pm |A_c| e^{i\Delta_c})$
- $A(B^- \to D^0_\pm K^{*-}) = \frac{1}{\sqrt{2}}(A(B^- \to D^0 K^{*-}) \pm A(B^- \to \overline{D^0} K^{*-})$
  $A(B^- \to D^0_\pm K^{*-}) = \frac{1}{\sqrt{2}}(|A_c| e^{i\Delta_c} \pm |A_u| e^{i(\Delta_u - \gamma)})$

The decay widths are deduced :

- $\Gamma(B^+ \to D^0_\pm K^{*+}) \alpha |A(B^+ \to D^0_\pm K^{*+})|^2$
  $\Gamma(B^+ \to D^0_\pm K^{*+}) = \frac{1}{2}(|A_u|^2 + |A_c|^2 + \pm |A_u||A_c|(e^{i(\Delta_u + \gamma - \Delta_c)} + e^{-i(\Delta_u + \gamma - \Delta_c)})$
  $\Gamma(B^+ \to D^0_\pm K^{*+}) = \frac{1}{2}|A_c|^2(1 + r_B^2 \pm 2 r_B cos(\delta_b + \gamma))$
  Where $\delta_B = \Delta_u - \Delta_c$ and $r_B = \frac{|A_u|}{|A_c|}$.
- $\Gamma(B^- \to D^0_\pm K^{*-}) \alpha |A(B^- \to D^0_\pm K^{*-})|^2$
  $\Gamma(B^- \to D^0_\pm K^{*-}) = \frac{1}{2}(|A_c|^2 + |A_u|^2 + \pm |A_c||A_u|(e^{i(\Delta_c + \gamma - \Delta_u)} + e^{-i(\Delta_c + \gamma - \Delta_u)})$
  $\Gamma(B^- \to D^0_\pm K^{*-}) = \frac{1}{2}|A_c|^2(1 + r_B^2 \pm 2 r_B cos(\delta_b - \gamma))$

- $\Gamma(B^+ \to D^0 K^{*+}) = |A_c|^2$

- $\Gamma(B^+ \to \overline{D^0} K^{*+}) = |A_c|^2$

Replacing the expressions of the decay widths in $R_{CP_\pm}$ and $A_{CP_\pm}$, one finds:

$$R_{CP_\pm} = 2\frac{\Gamma(B^- \to D^0_\pm K^{*-}) + \Gamma(B^+ \to D^0_\pm K^{*+})}{\Gamma(B^- \to D^0 K^{*-}) + \Gamma(B^+ \to \overline{D^0} K^{*+})} = 1 + r_B^2 \pm 2 r_B cos\delta_B cos\gamma$$

$$A_{CP_\pm} = \frac{\Gamma(B^- \to D^0_\pm K^{*-}) - \Gamma(B^+ \to D^0_\pm K^{*+})}{\Gamma(B^- \to D^0_\pm K^{*-}) + \Gamma(B^+ \to D^0_\pm K^{*+})} = \frac{\pm 2 r_B (cos(\delta_B + \gamma) - cos(\delta_B - \gamma)}{1 - r_B^2 \pm r_B (cos(\delta B + \gamma) + cos(\delta B - \gamma))}$$

$$A_{CP_\pm} = \frac{\pm 2 r_B sin\delta_B sin\gamma}{1 + r_B^2 \pm 2 r_B cos\delta_B cos\gamma}$$

ADS observables

Amplitudes of the D Doubly Cabibbo suppressed decays: $(D^0 \to f \ ; \ \overline{D^0} \to \overline{f})$
$A(D^0 \to f) = A(\overline{D^0} \to \overline{f}) = |A_f| e^{i\Delta_f} = r_D |A_{\overline{f}}| e^{-i\Delta_f} = r_D A_{\overline{f}} e^{-i\delta_D}$
Amplitudes of the D Cabibbo favored decays: $(\overline{D^0} \to f \ ; \ D^0 \to \overline{f})$
$A(D^0 \to \overline{f}) = A(\overline{D^0} \to \overline{f}) = A_{\overline{f}} = |A_{\overline{f}}| e^{i\Delta_{\overline{f}}}$
One can deduce :

- $A(B^+ \to D(\to \overline{f}) K^{*+}) = A(B^+ \to D^0 K^{*+}) A(D^0 \to \overline{f}) + A(B^+ \to \overline{D^0} K^{*+}) A(\overline{D^0} \to \overline{f})$
  $A(B^+ \to D(\to \overline{f}) K^{*+}) = r_B A_c A_{\overline{f}} e^{i(\delta_B + \gamma)} + r_D A_c A_{\overline{f}} e^{-i\delta_D} = A_c A_{\overline{f}} (r_B e^{i(\delta_B + \gamma} + r_D e^{-i(\delta_D)})$

- $A(B^- \to D(\to f) K^{*-}) = A(B^- \to D^0 K^{*-}) A(D^0 \to f) + A(B^- \to \overline{D^0} K^{*-}) A(\overline{D^0} \to f)$
  $A(B^- \to D(\to f) K^{*-}) = A_c A_{\overline{f}} (r_D e^{-i\delta_D} + r_B e^{i(\delta_B - \gamma)})$

- $A(B^+ \to D(\to f) K^{*+}) = A_c A_{\overline{f}} + r_B r_D A_c A_{\overline{f}} e^{i(\delta_B - \delta_D + \gamma)}$

- $A(B^- \to D(\to \overline{f}) K^{*-}) = A_c A_{\overline{f}} + r_B r_D A_c A_{\overline{f}} e^{i(\delta_B - \delta_D - \gamma)}$

  The decay widths are deduced :

- $\Gamma(B^- \to D(\to f) K^{*-}) \alpha |A_c|^2 |A_{\overline{f}}|^2 (r_D^2 + r_B^2 + r_B r_D (e^{i(\delta_B + \delta_D - \gamma} + (e^{-i(\delta_B + \delta_D - \gamma)})$
  $\Gamma(B^- \to D(\to f) K^{*-}) \alpha |A_c|^2 |A_{\overline{f}}|^2 (r_D^2 + r_B^2 + 2 r_D r_B cos(\delta_B + \delta_D - \gamma))$

- $\Gamma(B^+ \to D(\to \overline{f}) K^{*+}) \alpha |A_c|^2 |A_{\overline{f}}|^2 (r_D^2 + r_B^2 + 2 r_D r_B cos(\delta_B + \delta_D + \gamma))$
  $cos(\delta_B + \delta_D + \gamma) + cos(\delta_B + \delta_D - \gamma) = 2 cos(\delta_B + \delta_D) cos(\gamma)$
  $\Gamma(B^- \to D(\to f) K^{*-}) + \Gamma(B^+ \to D(\to \overline{f}) K^{*+}) = 2 |A_c|^2 |A_{\overline{f}}|^2 (r_B^2 + r_D^2 + 2 r_B r_D cos(\delta_B + \delta_D) cos\gamma)$

- $\Gamma(B^- \to D[\to \overline{f}]K^{*-})\alpha|A_c|^2|A_{\overline{f}}|^2(1 + r_B^2 r_D^2 + 2r_B r_D cos(\delta_B - \delta_D - \gamma))$

- $\Gamma(B^- \to D[\to f]K^{*-})\alpha|A_c|^2|A_{\overline{f}}|^2(1 + r_B^2 r_D^2 + 2r_B r_D cos(\delta_B - \delta_D + \gamma))$
  $\Gamma(B^- \to D[\to \overline{f}]K^{*-}) + \Gamma(B^- \to D[\to f]K^{*-}) \backsimeq 2|A_c|^2|A_{\overline{f}}|^2$

Replacing the expressions of the decay widths in R_{ADS} and A_{ADS}, one finds:

$$R_{ADS} = r_B^2 + r_D^2 + r_B r_D cos(\delta_B + \delta_D) cos\gamma$$

$$A_{ADS} = \frac{4r_B r_D |A_c^2||A_{\overline{f}}|^2 sin(\delta_B + \delta_D) cos\gamma}{2|A_c^2||A_{\overline{f}}|^2 R_{ADS}}$$

$$A_{ADS} = \frac{2r_B r_D sin(\delta_B + \delta_D) sin(\gamma)}{R_{ADS}}$$

B Appendix- Event selection

Table 4: The mass cut values [6]

Mass window	cut value (Gev/c^2)
$\lvert M(KsDD)_{PDG} - M(KsDD)\rvert$	> 0.01985
$\lvert M(KsLL)_{PDG} - M(KsLL)\rvert$	> 0.01105
$\lvert M(K^*)_{PDG} - M(K^*)\rvert$	> 0.1
$\lvert M(D)_{PDG} - M(D)\rvert$	> 0.02408
$\lvert M(B)_{PDG} - M(B)\rvert$	> 0.05334

Table 5: The selection cuts

Discriminating variable	Selection cut DD	Selection cut LL
χ2FD(Ks)	< 105	< 1000
$Log(DIRA_{Ks})$	<-10	<-10
$\frac{\Delta Z(Ks-B)}{\sqrt{\sigma_{Ks}^2 - \sigma_B^2}}$	< 7	< 63
PID RICH	< 0.1	<0.1
$cos(\theta_{Helicity_{K^*}})$	> 0.6	> 0.6
$\frac{\Delta Z(D-B)}{\sqrt{\sigma_D^2 - \sigma_B^2}}$	< 0	<0
Max DoCa	>0.1	>0.1
χ2FD(Ks DD)	<500	
$Log(DIRA_D)$		<-15
$P_T(D)$	<3	<3
$P_T(K*)$	<2	<2
$cos(\theta_{Helicity_{K^*}})$	> 0.6	>-0.4
χ2FD(B)	<500	<400
$Log(DIRA_B)$	>-14	>-12
χ2IP	>9	>6

The distributions of two discriminating variables the transverse momentum of D ($P_T(D)$) and χ^2 of the flight distance of B are presented in Figure 33,35 along with the significance Q in Figure 34,36.

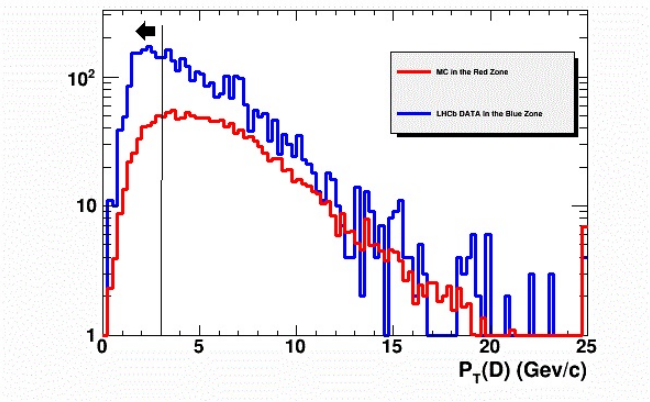

Figure 33: $P_T(D)$ distributions LL

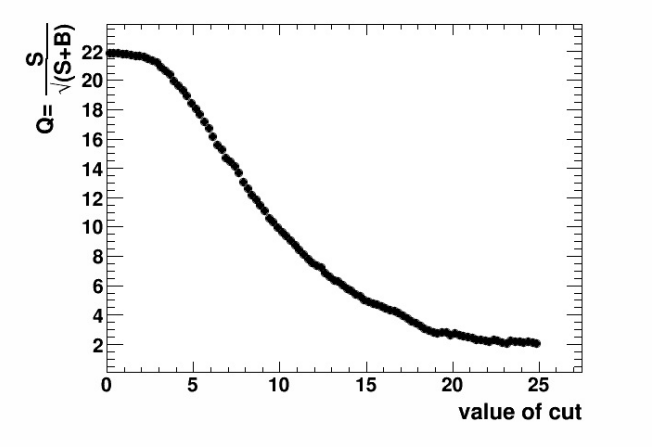

Figure 34: The significance Q

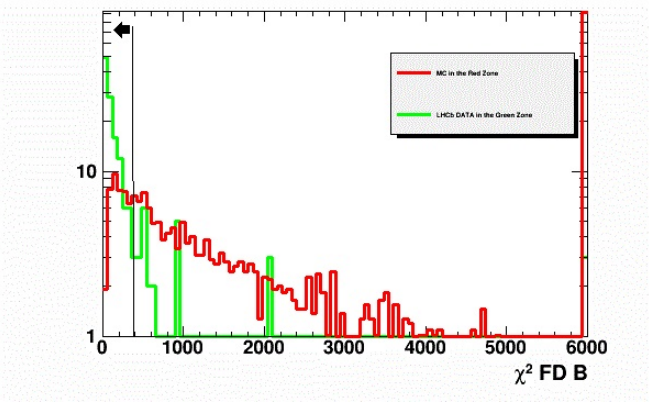

Figure 35: χ^2FD of B distributions DD

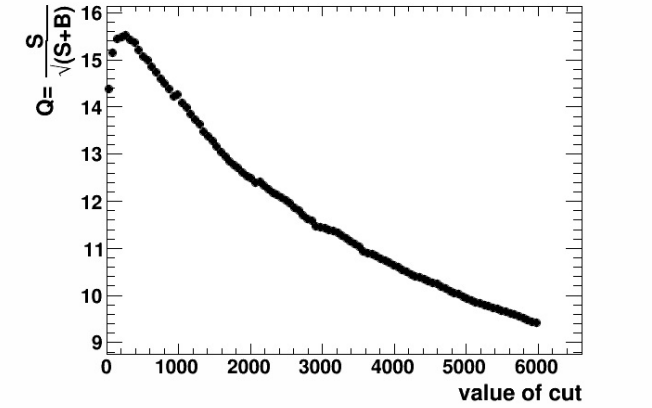

Figure 36: The significance Q

C Appendix-Particles properties

Table 6: Particles properties

Particle	Mass (Mev/c^2)	$P(Gev/c)$	Flight distance L	J^P	Branching ratios
B	5279.25 ± 0.26	140	$1.30cm$	0^-	$Br(B \to DK^*(891)) = (5.3 \pm 0.4) \times 10^{-4}$
D^0	$1864,86 \pm 0,13$	86	$5.6mm$	0^-	$Br(D \to \pi^+\pi-) = (1.402 \pm 0.026) \times 10^{-3}$ $Br(D \to K^+K^-) = (3.96 \pm 0.08) \times 10^{-3}$ $Br(D \to K^+\pi-) = (1.380 \pm 0.028) \times 10^{-4}$ $Br(D \to K^-\pi+) = (3.88 \pm 0.05) \times 10^{-2}$
K^*	891.66 ± 0.26	45	$3.48 \times 10^{-13}\mu m$	1^-	$Br(K^* \to K_s^0\pi) = 0.33$
K_s^0	$497,614 \pm 0,02$	29	$1.54m$	0^-	$Br(K_s^0 \to \pi^+\pi-) = (69.20 \pm 0.05) \times 10^{-2}$

The flight distance is determined for a typical momentum P using the following relation $L = \beta\gamma c\tau = \dfrac{P}{M}c\tau$ where τ is the lifetime of the particle.

References

[1] C. S. Wu, E. Ambler, R. W. Hayward, D. D. Hoppes, and R. P. Hudson, 1957, *Experimental Test of Parity Conservation in Beta Decay*. Phys. Rev. 105, 1413.

[2] J. Christenson, J. Cronin, V. Fitch and R. Turlay, Phys. Rev. Lett. 13, (1964).18

[3] B. Aubert et al. (BABAR), Phys. Rev. Lett. 87 (2001) 091801

[4] K. Abe et al.(Belle), Phys. Rev. Lett. 87 (2001) 091802

[5] S.L. Glashow, J. Iliopoulos, L. Maiani (1970)."Weak Interactions with Lepton Hadron Symmetry".Physical Review D 2 (7): 1285. Bibcode:1970PhRvD...2.1285G. doi:10.1103/PhysRevD.2.1285.

[6] M.Kobayashi, T.Maskawa : CP-Violation in the Renormalizable Theory of Weak Interaction, Progress of Theorical Physics 49, 652-657

[7] K.A. Olive et al. (Particle Data Group), Chin. Phys. C, 38, 090001 (2014).

[8] J. Charles, et al.,"Current status of the Standard Model CKM fit and constraints on $\Delta F = 2$ New Physics"

[9] http://ckmfitter.in2p3.fr/www/results/plots_ckm14/ckm_res_ckm14.html#ettiquette11

[10] M. Gronau and D. Wyler, Phys. Lett. B 265, 172 (1991)

[11] M. Gronau and D. London, Phys. Lett. B 253, 483 (1991)

[12] D. Atwood, I. Dunietz and A. Soni, Phys. Rev. Lett. 78 3257 (1997)

[13] http://arxiv.org/abs/1412.7515

[14] http://arxiv.org/abs/1412.6352

[15] http://lhcb-release-area.web.cern.ch/LHCb-release-area/DOC/gauss/generator/evtgen.php

[16] http://geant4.cern.ch/

[17] http://lhcb-release-area.web.cern.ch/LHCb-release-area/DOC/brunel/

[18] http://lhcb-release-area.web.cern.ch/LHCb-release-area/DOC/davinci/

[19] http://arxiv.org/pdf/1306.3663v2.pdf

[20] http://pdg.lbl.gov/2011/reviews/rpp2011-rev-monte-carlo-numbering.pdf

[21] L.Lyons, D.Gibaut and P.Clifford, How to combine correlated estimates of a single physical quantity, NIM A270(1988) 110

[22] arxiv.org/pdf/0909.3981.pdf

Abstract

This document presents, a preliminary study towards the measurement of the CKM angle γ through the tree level decay $B \to D[hh]K^*[K_s\pi]$ where $hh = K^+K^-, \pi^+\pi^-$ or $K\pi$. Using the LHCb data collected in 2011 2012 and the Monte Carlo simulation sample, a selection on discriminating variables has been preformed in order to purify the decay chain from the background events. Following the selection cuts, the reconstructed invariant mass distributions of the particles K_s, K^*, D, B were presented. The subsisting events were split based on D's final state and B's charge. Afterwards, they were used for the GLW and ADS methods where the CP violation observables A_{ADS}, R_{ADS}, A_{CP^+}, R_{CP^+} were measured experimentally.

Key words: LHCb, CKM angle γ, CP violation observables, selection, discriminating variables.

Resumé

Ce document présente, une étude préliminaire vers la mesure de l'angle CKM γ par la désintégration en arbre $B \to D[hh]K^*[K_s\pi]$ où $hh = K^+K^-, \pi^+\pi^-$ ou $K\pi$. En utilisant les données de LHCb rassemblées en 2011 2012 et l'échantillon de données de la simulation Monte Carlo, une sélection sur des différentes variables discriminantes a été préformée dans le but de purifier la chaîne de désintégration du bruit de fond. Après les coupures de sélection, les distributions de masse invariante reconstruite des particules K_s, K^*, D, B ont été présentées. Les événements restants ont été séparés en se basant sur l'état final du D et la charge de B. Ensuite, ils ont été utilisés pour les méthodes GLW et ADS où les observables de violation CP A_{ADS}, R_{ADS}, A_{CP^+}, R_{CP^+} ont été mesurées expérimentalement.

Mots clés: LHCb, angle CKM γ, observables de violation CP, sélection, variables discriminantes.